Scilight

Low-Dimensional Materials

https://www.sciltp.com/journals/ldm

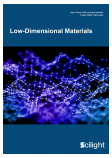

Article

Check for updates

Synthesis and Characterization of Ternary Metallic Oxide (Zn-Mn-AgO) Nanoparticles and Their Photocatalytic Degradation Performance for Malachite Green Dye

Muhammad Rahim [1], Shafeeq Ur Rahman [1], Shahab Khan [1,2,*], Kashif Iqbal [3] and Asad Ullah [1]

[1] Department of Chemistry, Government Ghazi Umara Khan Degree College, Samarbagh 18600, Pakistan
[2] Department of Chemistry, University of Malakand, Chakdara 18800, Pakistan
[3] Department of Chemical Engineering, Wah Engineering College, University of Wah, Wah 47040, Pakistan
* Correspondence: Shahabkhan262@gmail.com

How To Cite: Rahim, M.; Rahman, S.U.; Khan, S.; et al. Synthesis and Characterization of Ternary Metallic Oxide (Zn-Mn-AgO) Nanoparticles and Their Photocatalytic Degradation Performance for Malachite Green Dye. *Low-Dimensional Materials* **2026**, *2*(3), 10. https://doi.org/10.53941/ldm.2026.1000010

Received: 8 July 2026
Revised: 28 August 2026
Accepted: 9 September 2026
Published: 22 September 2026

Abstract: In this work, a Zn-Mn-AgO ternary metal oxide nanoparticle was prepared through a straightforward co-precipitation route and evaluated as a photocatalyst for degrading malachite green dye. We used Scanning electron microscopy (SEM), Fourier-transform infrared spectroscopy (FTIR), X-ray diffraction (XRD), and energy-dispersive X-ray spectroscopy (EDX) to characterize the trimetallic oxide nanoparticles (NPs). The SEM images reveal a spherical, dense, and agglomerated particle morphology. The average particle size was estimated at 51 nm using ImageJ software (version 1.53t, National Institutes of Health, USA). The results confirm the formation of ternary metal oxide nanoparticles (Zn-Mn-AgO NPs). About 93–95.26% degradation of the selected dye was calculated within 125 min. The effect of time, pH, and concentration was also studied.

Keywords: photocatalytic recycling stability; degradation of malachite green; Zn-Mn-AgO NPs; oxidative degradation

1. Introduction

The term “nano” originates from a Greek word meaning extremely small and refers to a scale of one billionth of a meter (10^{-9} m). Nanoscience focuses on the study of materials, and molecules at the nanoscale, which generally ranges from 1 to 100 nanometers (nm). At this scale, materials often exhibit unique physical, chemical, and biological properties that differ from their bulk counterparts [1]. Nanoscience sits at the intersection of chemistry and nanotechnology, and has emerged as a distinct branch of solid-state chemistry focused on developing preparation methods for materials with nanometer-scale dimensions. It centers on the synthesis of building blocks whose properties depend on size, surface characteristics, shape, and defects, and it finds use across chemical, materials, physical, engineering, biological, and medical fields. While nanotechnology shares core concepts with other nanoscience disciplines, the way these concepts are applied differs between fields [2].

Nanotechnology, often shortened to nanotech, is concerned with manipulating matter at the atomic, molecular, and supramolecular scale for a wide range of industrial uses. Early definitions of the field centered on the goal of precisely arranging atoms and molecules to build macroscale products, an approach later labeled molecular nanotechnology [3,4]. Nanoscience, as a broader discipline, therefore spans both nanotechnology and nanochemistry. A central goal of nanotechnology is designing nanoparticles (NPs) with novel properties and building materials and devices around them, making it one of the defining research areas of twenty-first-century science. Nanochemistry’s development reflects a shift from micro-scale to nano-scale study; investigating

nanosized particles uncovered size-dependent effects that add a new dimension to material properties and give rise to chemical transformations not seen before. Early research in this area concentrated on atoms, clusters, and NPs of various metals, along with semiconductors, fullerenes, and carbon nanotubes, and the physicochemical behavior of these materials laid the groundwork for the field of nanotechnology [5]. Nanotechnology now finds application across science, agriculture, food, medicine, pharmaceuticals, and energy, contributing to more durable construction materials, targeted drug delivery, and cleaner high-density hydrogen fuel cells. Because of their favorable physicochemical properties, NPs and nanodevices are also employed in nanoelectronics, cancer therapy, vaccine development, hydrogen fuel cells, and graphene-based batteries. Mehdi F. et al. reported that zero-valent iron nanoparticles are also efficient for the removal of Cr from aqueous media [6]. By working with smaller-scale materials, nanotechnology allows subtle modification of molecules and substances, which can improve the catalytic performance as well [7]. In cancer treatment, nanotubes have shown effectiveness at destroying tumors in kidney and breast cancer patients [8,9]. Ultra-black materials, formed from dense "forests" of carbon nanotubes, are valuable in space applications and can be incorporated into cameras and telescopes to reduce stray light and sharpen captured images [10]. Nanotubes are also being explored for cardiovascular treatment, where they may assist in clearing blood vessels [11], and for body armor, where their strength could effectively shield soldiers from projectiles and electromagnetic radiation [12].

Because nanotechnology allows materials to be observed and engineered at the nanoscale, it has considerable potential in construction, where it can improve the strength and durability of cement [13], steel, wood, and glass. In electronics, nanotechnology is used to boost display performance and reduce power consumption while making components smaller [8], and nanoelectronics itself draws on quantum physics, device analysis, system integration, and circuit design [14]. The related fields of nano-biotechnology and bio-nanotechnology bring together ideas, methods, and knowledge from biology and nanotechnology, the former applying nanoscale tools to biotechnology, the latter incorporating biological components into nanotechnology. Their most notable convergence is in nanomedicine, where NPs and nanodevices support drug delivery, health monitoring, and disease diagnosis. NPs are also used as contrast agents in *in vivo* imaging techniques such as CT, MRI, and PET scans, making them valuable for nanomedicine [15]. Energy is another area where nanotechnology plays a role, since the small size of NPs allows energy to be stored more efficiently. This supports green nanotechnology's goal of generating, storing, and using energy without releasing greenhouse gases such as carbon dioxide, and NPs incorporated into solar cells help capture more energy from sunlight [16]. Conventional solar cells rely on silicon layers to absorb sunlight and convert it into electricity, but much of that energy is lost as heat; incorporating NPs reduces this heat loss and improves electricity output [17]. Zinc oxide NPs in particular are widely applied in microelectronics, diagnostics, optoelectronic devices, biomolecular sensing, surface acoustic wave devices, lasers, and electromagnetic coupling sensors [18], and can also serve as an alternative means of breaking down atmospheric pollutants [19,20]. Water, essential to all life on Earth, holds unmatched importance [21], yet worldwide water pollution is intensifying due to rapid industrial growth, population increase, and shifting climate patterns [22]. Projections suggest that by 2025 nearly half of the global population could face freshwater shortages, with that figure potentially rising to around 75% by 2075 [23], underscoring water's essential role in sustaining global economic stability [24]. Existing water conservation efforts, while important, have not been sufficient to curb this shortage [25]. Wastewater treatment is particularly critical in water-intensive, pollution-heavy industries such as textiles; producing just 0.5 kg of textile goods can require roughly 80 L of water [26], and the textile sector alone is estimated to discharge around 2% of all dyes into water systems, creating health and environmental hazards [27,28]. Dyes released from textile dyeing, paper, paint, cosmetics, and food processing tend to resist breakdown and can generate harmful by-products during treatment [29]. Dyes are broadly grouped into natural and synthetic types, with azo compounds accounting for over half of synthetic industrial dyes and behaving as cationic, anionic, or non-ionic species depending on pH [30]. Methylene blue and malachite green are common synthetic dyes used in textile and paper dyeing as well as in medical treatments [31]; methylene blue, for instance, is used medically to treat neuro-inflammation, oxidative stress, nausea, and gastrointestinal infections [32]. Given these hazards, removing such dyes from water is essential [33]. A range of methods has been developed for synthetic dye removal, including adsorption, Fenton-like reactions with activated sludge, membrane filtration, and photocatalysis [34–40]. Photocatalysis in particular uses semiconductor NPs to convert solar energy into a driving force for dye breakdown and mineralization [41]: photon absorption above the semiconductor's band gap generates an electron-hole pair that drives redox reactions at the catalyst surface, producing superoxide and hydroxyl radicals that oxidize organic dye molecules [42]. In recent years, the contamination of water resources by synthetic dyes has become a serious environmental concern due to their high toxicity, carcinogenic nature, and persistence in aquatic ecosystems [43]. Among various organic dyes, malachite green dye is widely used in the textile, paper, and leather industries; however, its discharge into water bodies poses significant risks to human health and aquatic life. Conventional wastewater treatment methods such

as adsorption, ref. [44] coagulation, and biological treatment often fail to completely degrade such stable dye molecules. Therefore, advanced photocatalysis has emerged as a promising alternative for the removal of recalcitrant organic pollutants. Semiconductor photocatalysts like ZnO and MnO_2 have attracted considerable attention because of their low cost, chemical stability, and strong capability [45]. However, their photocatalytic efficiency is limited by a wide band gap and rapid recombination of photogenerated electron-hole pairs. To overcome these limitations, the coupling of zinc oxide and MnO with noble metals such as silver has been proposed as an effective strategy [46]. The incorporation of doping ions can also tune the dielectric, magnetic, and optical properties of host materials [47]. Several studies have reported that binary systems like Ag-ZnO [48]. The Ag-ZnO exhibit improved photocatalytic activity for dye degradation [49]. Recent reviews have highlighted that ternary metal oxide nanocomposites demonstrate superior performance compared to single and binary catalysts for wastewater treatment [50]. Despite several reports on ZnO and MnO-based photocatalysts, there are still some limitations, such as very high charge carrier recombination rates and low visible light absorption. To overcome these issues, the present work reports the synthesis of novel ternary metal oxide NPs of Zn-Mn-AgO via the co-precipitation method. The incorporation of Ag NPs is expected to enhance the charge separation and extend the light absorption to the visible region due to the surface plasmon resonance effect [51]. Furthermore, the coupling of ZnO with MnO_2 forms a heterojunction which further suppresses the recombination of electron-hole pairs [52]. The photocatalytic application of the synthesized NPs was evaluated for the degradation of malachite green dye under visible light irradiation; therefore, this work provides a new efficient and cost-effective photocatalyst for the removal of toxic dyes from wastewater.

2. Experimental Work

2.1. Chemicals and Reagents

All chemicals used in this study were of analytical grade and utilized without further purification. Zinc sulfate heptahydrate ($ZnSO_4 \cdot 7H_2O$, 99%) was purchased from Merck KGaA, Darmstadt, Germany. Manganese sulfate ($MnSO_4$, 99.8%) was obtained from BDH Laboratory Supplies, Poole, England, while silver nitrate ($AgNO_3$, 99.8%) and sodium hydroxide (NaOH, 99%) were supplied by Sigma-Aldrich (St. Louis, MO, USA). Ethanol (C_2H_5OH) and distilled water were used as solvents during the synthesis and washing processes. Malachite green (MG) dye was purchased from Danyal Trading Company and used as a model organic pollutant for photocatalytic degradation studies.

2.2. Characterization Techniques

The structural and surface properties of the synthesized Zn-Mn-AgO NPs were investigated using different analytical techniques. Fourier-transform infrared spectroscopy (FTIR) was employed to identify the surface functional groups and metal–oxygen bonding characteristics of the NPs within the range of 400–4400 cm^{-1}. FTIR analysis was performed at Bacha Khan University, Charsadda, Pakistan. The morphology, particle size, and surface characteristics of the synthesized NPs were examined using scanning electron microscopy (SEM) (ZEISS EVO 15, Carl Zeiss Microscopy GmbH, Jena, Germany). SEM analysis was carried out by scanning the nanoparticle surface with a focused electron beam, providing high-resolution information regarding particle shape and aggregation behavior. The elemental composition and chemical purity of the synthesized NPs were analyzed using energy-dispersive X-ray spectroscopy (EDX) coupled with an X-ray spectrometer (AXRD-LPD, Serial No. 20115300321). EDX analysis was used to determine the elemental constituents, as well as their corresponding weight and atomic percentages, confirming the presence of Zn, Mn, Ag, and O elements in the synthesized nanomaterial.

2.3. Synthesis of Zn-Mn-AgO NPs

The Zn-Mn-AgO NPs were synthesized through a co-precipitation method. Briefly, 100 mL of 0.1 mol m^{-3} $ZnSO_4$ solution, 100 mL of 0.1 mol m^{-3} $MnSO_4$ solution, and 100 mL of 0.1 mol m^{-3} $AgNO_3$ solution were mixed in a round-bottom flask under continuous magnetic stirring to obtain a homogeneous precursor solution. Subsequently, 0.2 mol m^{-3} NaOH solution was added dropwise under vigorous stirring until the pH of the reaction mixture reached approximately 10, promoting the precipitation of metal hydroxide intermediates. The resulting suspension was heated at 60 °C for 2 h under constant stirring to facilitate nucleation, growth, and formation of the Zn-Mn-AgO nanostructure. After completion of the reaction, the mixture was allowed to cool to room temperature, and the precipitated NPs were collected by filtration and repeatedly washed with distilled water to remove residual ions and unreacted precursors. Finally, the obtained Zn-Mn-AgO NPs were dried under controlled conditions and stored for further characterization and photocatalytic studies.

2.4. Photodegradation of Malachite Green Dye by Utilizing Zn-Mn-AgO NPs

The synthesized Zn-Mn-AgO NPs were tested as a sunlight-driven photocatalyst for degrading malachite green (MG) dye. A 0.025 kg m^{-3} MG dye solution was prepared, and 20 mL portions of this solution were placed in 50 mL beakers along with 0.0001 g of the catalyst NPs. Each sample was kept in the dark for 20 min to reach adsorption-desorption equilibrium before being exposed to sunlight under continuous stirring for different irradiation times. After irradiation, the catalyst was filtered out of the solution, and a UV-visible spectrophotometer (Shimadzu UV-1800, Shimadzu Corporation, Kyoto, Japan) was used to monitor the extent of MG dye degradation. The photodegradation behavior of MG was assessed as a function of catalyst dose, catalyst recovery and reuse, dye concentration, irradiation time, and solution pH. Catalyst-dose experiments varied the amount of catalyst while holding all other parameters fixed. For the pH study, solutions at pH 4, 7, and 10 were prepared using the addition of 0.1 mol m^{-3} HNO_3 for the acidic solution and dropwise addition of 0.1 mol m^{-3} NaOH to distilled water for the basic solution to evaluate how pH affects dye photodegradation. In the time-based study, dye solutions were irradiated for 25, 50, 75, 100, and 125 min with all other conditions kept constant, while the concentration study photodegraded solutions of 0.090, 0.100, 0.110, 0.120, and 0.130 kg m^{-3} under other fixed conditions.

3. Results and Discussion

3.1. FTIR Analysis and XRD

The FTIR spectrum of the synthesized Zn-Mn-AgO NPs (NPs) provides evidence for the formation of metal oxide bonds and surface functional groups associated with nanoparticle synthesis. The strong absorption band observed at 563 cm^{-1} is attributed to metal-oxygen stretching vibrations, mainly related to Zn–O/Mn–O/Ag–O lattice vibrations, confirming the formation of the mixed metal oxide nanostructure. Similar low-wavenumber metal-oxygen bands are commonly reported as fingerprints for metal oxide NPs. The presence of Mn and Ag ions within the ZnO matrix may cause slight shifts in the metal–oxygen vibration region due to lattice distortion, defect formation, and changes in bond strength caused by dopant incorporation. The peak around 1360 cm^{-1} can be associated with residual carbonate/nitrate species or surface-adsorbed oxygen-containing groups originating from the precursor materials or synthesis medium. The band at 1631 cm^{-1} corresponds to O–H bending vibrations of adsorbed water molecules, indicating the presence of hydroxyl groups on the nanoparticle surface. These surface hydroxyl groups are commonly observed in metal oxide NPs and can contribute to surface reactivity and stabilization of NPs. The absence of strong organic functional group peaks suggests effective removal or decomposition of precursor residues during synthesis.

The XRD pattern of the synthesized Zn-Mn-AgO NPs is shown in Figure 1b, where PDF 87-597 was used as a standard. This figure displays a prominent diffraction peak near a 2θ value of approximately 38°, corresponding to the (1, 1, 1) plane of metallic silver. A second peak near 44° is attributed to the (2, 0, 0) plane of a manganese oxide phase such as MnO or Mn_3O_4, a phase that typically diffracts in this region. Peaks at 63° and 78° correspond to the (2, 2, 0), and (3, 1, 1) planes of zinc oxide, confirming the presence of crystalline ZnO within the composite. Together, these characteristic peaks confirm the successful formation of a trimetallic Zn-Mn-AgO with high crystallinity.

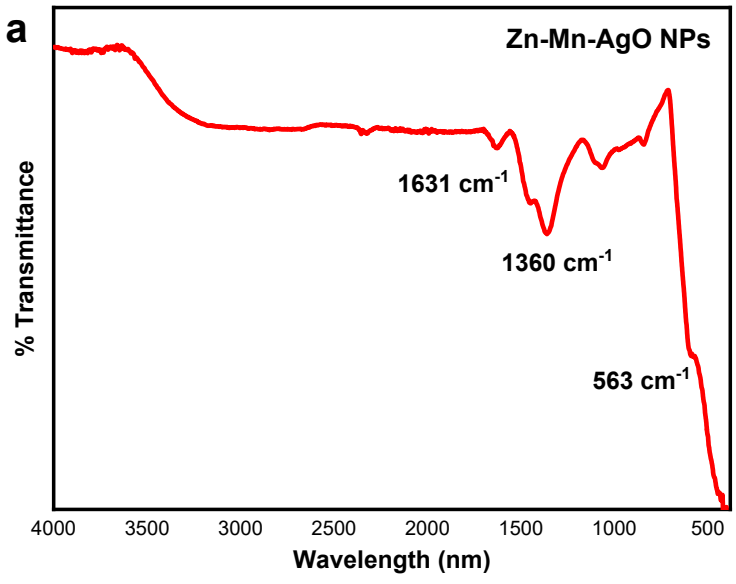

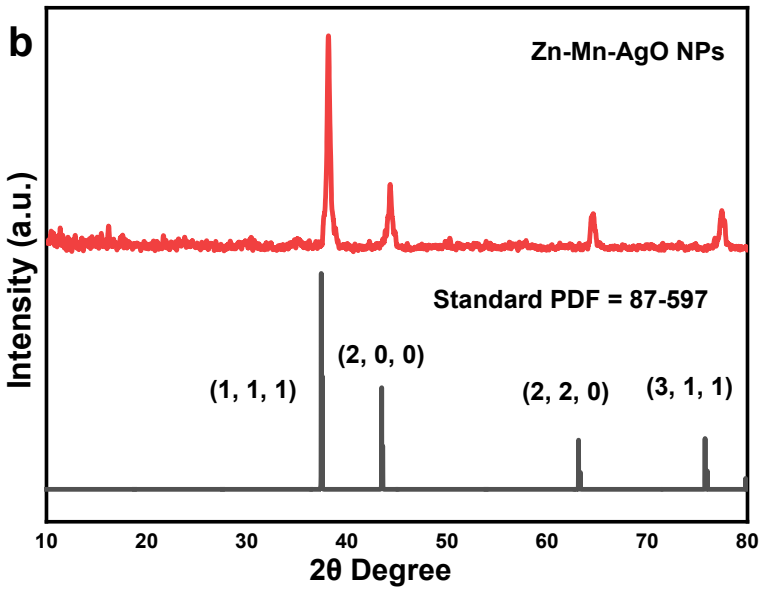

Figure 1. (**a**) FTIR analysis of Zn-Mn-AgO NPs. (**b**) X-ray diffraction analysis of Zn-Mn-AgO NPs.

3.2. EDX and SEM of Zn-Mn-AgO NPs

Energy-dispersive X-ray spectroscopy (EDX) analysis was performed to investigate the elemental composition and verify the successful formation of Zn-Mn-AgO NPs. The EDX spectrum (Figure 2a) reveals the characteristic peaks corresponding to Zn, Mn, Ag, and O elements, confirming the incorporation of all constituent elements within the synthesized ternary metal oxide nanostructure. The quantitative analysis indicates that the synthesized Zn-Mn-AgO NPs consist of Zn, Mn, Ag, and O with weight percentages of 19.96%, 18.35%, 28.45%, and 33.24%, respectively. The corresponding atomic percentages were determined to be 10.24%, 11.21%, 8.85%, and 69.70% for Zn, Mn, Ag, and O, respectively. The predominance of oxygen in the atomic composition is attributed to the oxide nature of the synthesized NPs, while the presence of Zn, Mn, and Ag signals confirms the successful doping/integration of metallic species into the oxide matrix. No additional elemental peaks associated with significant impurities were detected, demonstrating the high purity of the prepared NPs.

The surface morphology and particle characteristics of the Zn-Mn-AgO NPs were further examined using scanning electron microscopy (SEM), as presented in Figure 2b–e. The SEM micrographs reveal that the NPs exhibit a predominantly spherical morphology with a tendency toward agglomeration, which is commonly observed in nanoscale metal oxide materials due to high surface energy and interparticle interactions. The observed particles possess an average size of approximately 51 nm, confirming the formation of nanosized structures. The uniform distribution of NPs and the absence of large irregular particles indicate that the applied synthesis approach effectively controlled particle growth and produced well-defined Zn-Mn-AgO nanostructures.

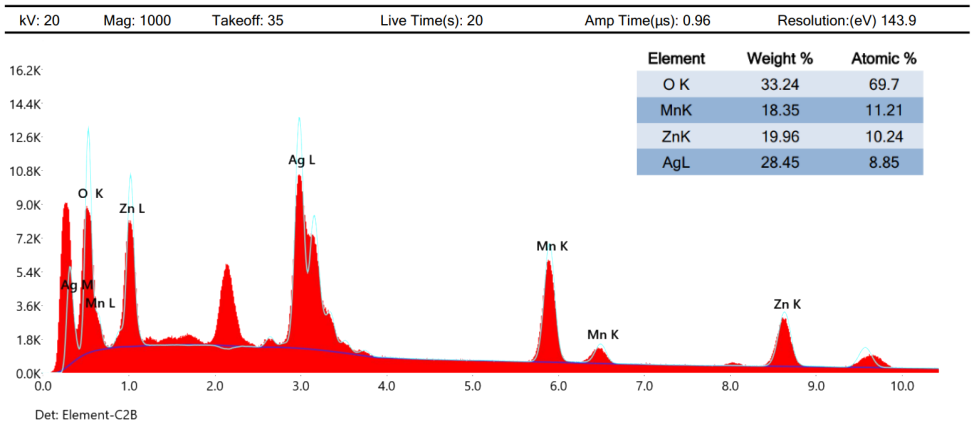

(**a**)

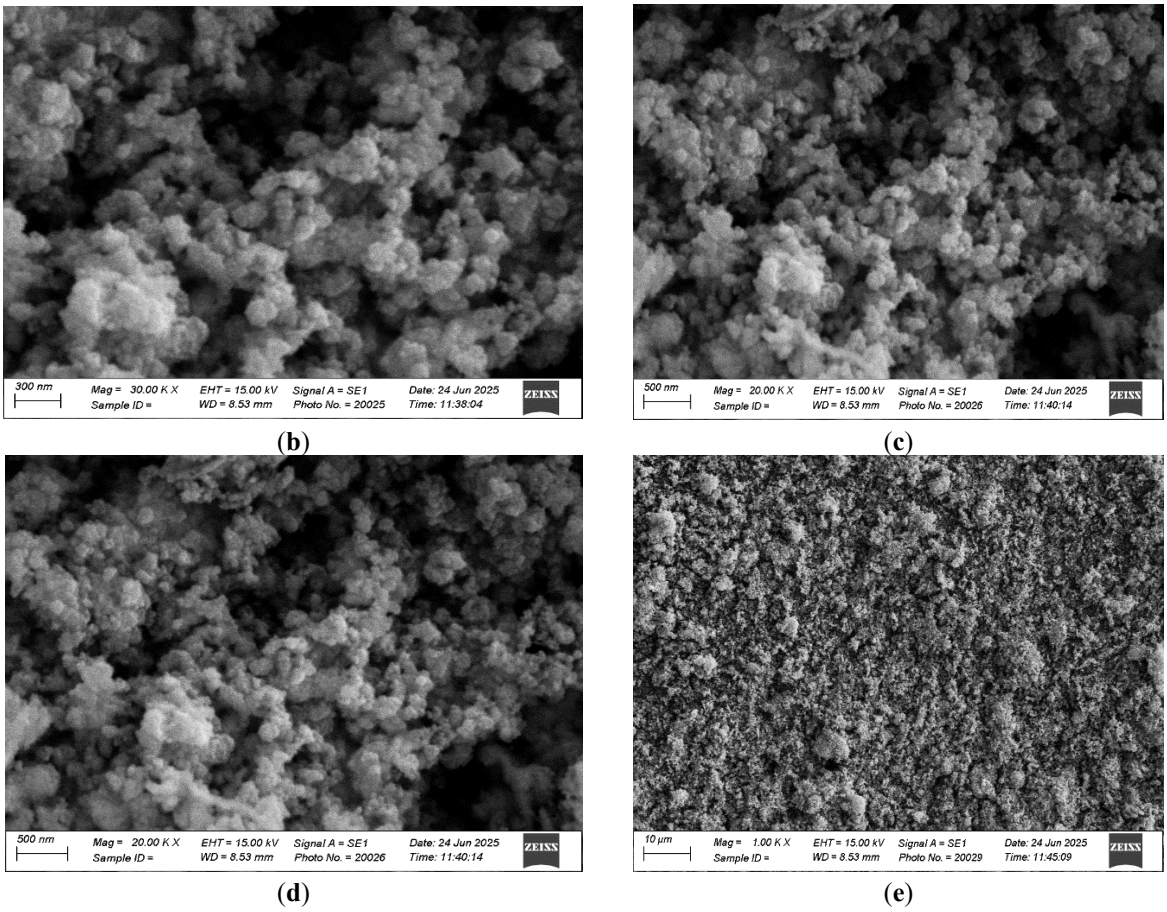

Figure 2. EDX and SEM. (**a**) EDX Spectrum of Zn-Mn-AgO NPs. (**b**–**e**) SEM images of Zn-Mn-AgO NPs.

3.3. Photocatalytic Degradation Activity of Malachite Green Dye Using Zn-Mn-AgO NPs

The photocatalytic performance of the synthesized Zn-Mn-AgO NPs was evaluated by studying the degradation of malachite green (MG) dye under sunlight irradiation. The enhanced photocatalytic activity of metal oxide nanomaterials is generally attributed to their semiconductor properties, where light irradiation generates electron–hole pairs. These photogenerated charge carriers participate in redox reactions with surface-adsorbed oxygen and water molecules, producing reactive oxygen species (ROS), mainly hydroxyl radicals ($\bullet OH^-$) and superoxide radicals ($\bullet O_2^-$), which are responsible for the oxidative degradation of organic dye molecules. The incorporation of Mn and Ag into ZnO-based systems can improve photocatalytic efficiency by modifying charge separation behavior, reducing electron-hole recombination, and providing additional active sites.

3.4. Effect of Irradiation Time on Photocatalytic Degradation

The influence of irradiation time on MG degradation was investigated using a dye concentration of 0.110 kg m^{-3} with a fixed amount of Zn-Mn-AgO photocatalyst. As shown in Figure 3a, the degradation efficiency increased continuously with increasing irradiation time. The degradation percentages were calculated as 31.57, 47.89, 64.21, 84.21, and 95.26% after 25, 50, 75, 100, and 125 min of irradiation, respectively. The gradual enhancement in degradation efficiency can be attributed to the increased interaction time between MG molecules and the photocatalyst surface, allowing greater generation and utilization of photogenerated reactive species. At longer irradiation periods, more dye molecules undergo oxidation due to prolonged exposure to ROS, resulting in improved degradation efficiency. The near-complete removal of MG after 125 min indicates the high photocatalytic activity of the synthesized Zn-Mn-AgO NPs.

3.5. Effect of Initial Dye Concentration on Photocatalytic Degradation

The effect of initial MG concentration on photocatalytic performance was examined by varying the dye concentration from 0.090 to 0.130 kg m^{-3} while maintaining a constant catalyst dosage (0.0004 g) and irradiation time (75 min). As presented in Figure 3b, the degradation efficiency decreased with increasing dye concentration, showing degradation values of 77, 74, 65, 55, and 32% for 0.090, 0.100, 0.110, 0.120, and 0.130 kg m^{-3} MG

solutions, respectively. This reduction can be explained by the increased number of dye molecules competing for adsorption sites on the photocatalyst surface. Furthermore, at higher dye concentrations, MG molecules can absorb a significant fraction of the incident light, reducing photon penetration into the catalyst suspension and limiting the formation of photogenerated electron–hole pairs. Consequently, fewer ROS are generated, resulting in reduced photocatalytic degradation efficiency. This behavior agrees with the commonly reported concentration-dependent photocatalytic degradation mechanism of semiconductor-based catalysts.

3.6. Effect of pH on Photocatalytic Degradation

The solution pH is an important parameter controlling photocatalytic dye degradation because it influences both the surface charge of the catalyst and the formation of reactive oxygen species. The effect of pH on MG degradation was studied under acidic (pH 4), neutral (pH 7), and alkaline (pH 10) conditions, and the results are presented in Figure 3c. The degradation efficiency increased from 58% at pH 4 to 64% at pH 7 and 75% at pH 10 after 75 min of irradiation. The improved degradation under alkaline conditions may be related to the higher availability of hydroxide ions (OH^-), which can react with photogenerated holes (h^+) to produce additional hydroxyl radicals (•OH), enhancing oxidative degradation of MG molecules. In addition, the surface charge characteristics of Zn-Mn-AgO NPs may promote stronger electrostatic interactions with the cationic MG dye under alkaline conditions, facilitating adsorption and subsequent degradation. Similar pH-dependent enhancement has been widely reported for ZnO-based photocatalysts.

3.7. Photocatalytic Recycling Stability of Zn-Mn-AgO NPs

The reusability of the synthesized photocatalyst was evaluated by comparing the photocatalytic performance of fresh and recovered Zn-Mn-AgO NPs under identical experimental conditions. As shown in Figure 3d, the fresh catalyst achieved approximately 95.26% degradation, whereas the recovered catalyst retained 84.21% degradation efficiency. The slight decrease in activity after recycling can be attributed to partial coverage of active surface sites by residual dye molecules, incomplete removal of intermediates, or minor structural changes during recovery and washing processes. Nevertheless, the recovered catalyst maintained a high degradation efficiency, demonstrating good stability and recyclability of Zn-Mn-AgO NPs. The retention of photocatalytic activity confirms that the synthesized material possesses potential for repeated application in wastewater treatment.

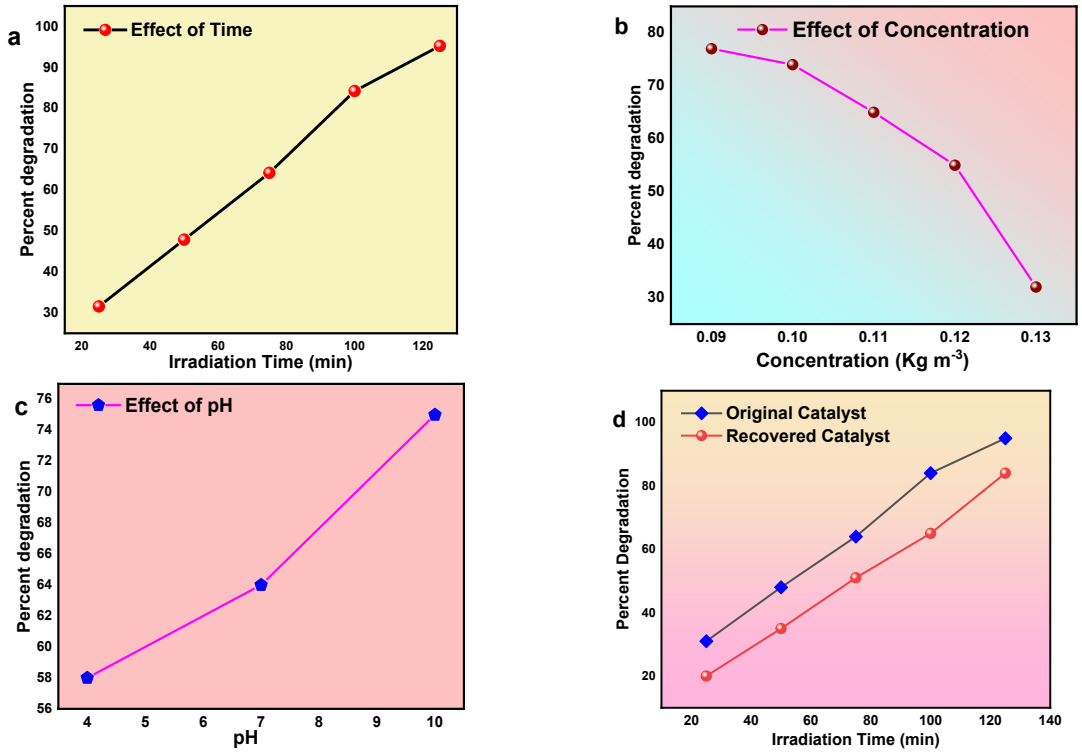

Figure 3. Optimization parameters and recyclability evaluation of Zn-Mn-AgO NPs for photocatalytic degradation of malachite green dye: (**a**) degradation efficiency as a function of irradiation time, (**b**) effect of initial MG concentration on degradation efficiency, (**c**) effect of pH variation on photocatalytic performance, and (**d**) comparison of degradation efficiency of original and recovered catalyst Zn-Mn-AgO NPs under identical irradiation conditions.

4. Conclusions

This study successfully synthesized trimetallic zinc-manganese-silver oxide (Zn-Mn-AgO) NPs using a simple and effective co-precipitation method. The prepared NPs were successfully formed, with good composition and suitable structural properties. The synthesis process is efficient. It is also practical. It provides a simple approach for producing advanced trimetal oxide nanomaterials. The formation of Zn-Mn-AgONPs was confirmed using various analytical techniques. FTIR analysis provided clear evidence of metal-oxygen bonds. The observed functional groups were associated with the structures of ZnO, MnO, and AgO. These results confirmed the presence of metal oxide bonds in the synthesized nanocomposites. FTIR results supported successful interactions among the three metal oxide components. They also indicated the presence of stable oxide-based nanomaterials. The crystalline properties of the synthesized NPs were confirmed by XRD analysis. The diffraction pattern showed strong and clear peaks. These peaks corresponded to the various oxide phases of zinc, manganese, and silver. The results showed that the NPs exhibited high crystallinity. The presence of characteristic diffraction peaks also confirmed the successful combination of zinc, manganese, and alumina components. This proved that the co-precipitation method is highly effective in preparing high-quality trimetal oxide NPs. EDX analysis further confirmed the elemental composition of the synthetic materials. The presence of zinc, manganese, silver, and oxygen was detected in the NPs. These results confirmed that all expected elements were successfully incorporated into the nanocomposites. The uniform combination of these elements promoted improved performance of the Zn-Mn-AgO NPs system. It also supported the successful preparation of targeted trimetallic NPs.

The surface morphology of synthesized NPs was analyzed using scanning electron microscopy. The images show that the NPs are mainly spherical. The average particle size is about 51 nanometers. This value is calculated using ImageJ software. The nanoscale size and spherical structure provide a large surface area. This characteristic is very important for enhancing catalytic activity. It allows more active sites to interact with pollutants during photocatalytic reactions. By degrading malachite green (MG) dye under sunlight, the photocatalytic activity of Zn-Mn-AgO NPs was evaluated. The results showed that the synthesized nanocatalyst exhibited excellent photocatalytic efficiency. The catalyst can effectively remove organic dyes from water. Different experimental conditions were studied. These conditions included catalyst dosage, dye concentration, pH value, and irradiation time. The study detailed the factors affecting the photocatalytic process. Zn-Mn-AgO NPs maintain strong performance under different working conditions. This consistency demonstrates the stability and reliability of nanocatalysts. Their ability to operate efficiently under sunlight is a significant advantage. It reduces dependence on artificial energy sources. At the same time, it makes the treatment process more economical and environmentally friendly. Therefore, synthetic nanomaterials have strong potential in practical applications in wastewater treatment. The successful degradation of malachite green highlights the environmental importance of this trimetallic oxide system. Malachite green is a harmful synthetic dye. It can pose serious risks to aquatic environments and human health. The developed Zn-Mn-AgO NPs provide an effective method for removing such pollutants from polluted water bodies. Using sunlight as a driving energy source further enhances the sustainability of this technology.

Additionally, this study explores the regenerative capabilities of catalysts. Regeneration research provides valuable information about the possibility of repeated use. Catalyst recycling and reuse are important factors for long-term application. Reusable catalysts can reduce operating costs. At the same time, they can minimize waste generation. Therefore, the regenerative potential of Zn-Mn-AgO NPs enhances their practical value in large-scale environmental remediation. This study shows that zinc-rice-nickel-nitrogen oxide NPs are promising materials for wastewater purification. Their simple synthesis process, strong structural properties, effective photocatalytic activity, and regenerative capabilities make these nanocomposites extremely valuable. The study proposes a sustainable solution for removing synthetic dyes in water. The developed trimetal oxide NPs bring hope for ongoing efforts to protect water resources. Amid the increasing challenges of water pollution, these nanomaterials offer promising directions for cleaner and safer environmental management.

Author Contributions

M.R.: Experimental work, conceptualization, methodology, software; S.U.R.: Data curation, writing—original draft preparation; A.U.: Visualization, investigation; S.K.: Supervision, writing—reviewing and editing; K.I.: Software, validation; All authors have read and agreed to the published version of the manuscript.

Funding

This research received no external funding.

Institutional Review Board Statement

Not applicable.

Informed Consent Statement

Not applicable.

Data Availability Statement

Data are available from the corresponding author upon reasonable request.

Conflicts of Interest

The authors declare no conflict of interest.

Use of AI and AI-Assisted Technologies

During the preparation and revision of this manuscript, ChatGPT (5.6-Sol) and Grammarly were used only for language polishing, grammar correction, and improving the clarity and readability of the text. No AI tools were used for generating scientific content, designing experiments, analyzing data, interpreting results, preparing images, or creating schematic illustrations. All experimental data, images, figures, and schematic diagrams presented in this manuscript are original and were prepared by the authors. The authors reviewed and edited all AI-assisted text and take full responsibility for the accuracy, integrity, and content of the final manuscript.

References

1. Gour, A.; Jain, N.K. Advances in green synthesis of nanoparticles. *Artif. Cells Nanomed. Biotechnol.* **2019**, *47*, 844–851. https://doi.org/10.1080/21691401.2019.1577878.
2. Chen, P.; Li, H.; Song, S.; et al. Adsorption of dodecylamine hydrochloride on graphene oxide in water. *Results Phys.* **2017**, *7*, 2281–2288. https://doi.org/10.1016/j.rinp.2017.06.054.
3. de Jesús Ruíz-Baltazar, Á.; Reyes-López, S.Y.; Pérez, R. Magnetic structures synthesized by controlled oxidative etching: Structural characterization and magnetic behavior. *Results Phys.* **2017**, *7*, 1828–1832. https://doi.org/10.1016/j.rinp.2017.05.001.
4. Baskakov, A.; Soloveva, A.; Ioni, Y.; et al. Magnetic and interface properties of the core-shell Fe_3O_4/Au nanocomposites. *Appl. Surf. Sci.* **2017**, *422*, 638–644. https://doi.org/10.1016/j.apsusc.2017.06.029.
5. Mohammadiyan, E.; Ghafuri, H.; Kakanejadifard, A. Synthesis and characterization of a magnetic Fe_3O_4@CeO_2 nanocomposite decorated with Ag nanoparticle and investigation of synergistic effects of Ag on photocatalytic activity. *Optik* **2018**, *166*, 39–48. https://doi.org/10.1016/j.ijleo.2018.03.044.
6. Fazlzadeh, M.; Rahmani, K.; Zarei, A.; et al. A novel green synthesis of zero valent iron nanoparticles (NZVI) using three plant extracts and their efficient application for removal of Cr (VI) from aqueous solutions. *Adv. Powder Technol.* **2017**, *28*, 122–130. https://doi.org/10.1016/j.apt.2016.09.003.
7. Khan, S.; Ullah, I.; Khan, H.; et al. Green synthesis of AgNPs from leaves extract of Salvia sclarea, their characterization, antibacterial activity, and catalytic reduction ability. *Z. Phys. Chem.* **2024**, *238*, 931–947. https://doi.org/10.1515/zpch-2023-0363.
8. Buzea, C.; Pacheco, I.I.; Robbie, K. Nanomaterials and nanoparticles: Sources and toxicity. *Biointerphases* **2007**, *2*, MR17–MR71. https://doi.org/10.1116/1.2815690.
9. Ji, S.R.; Liu, C.; Zhang, B.; et al. Carbon nanotubes in cancer diagnosis and therapy. *Biochim. Biophys. Acta Rev. Cancer* **2010**, *1806*, 29–35. https://doi.org/10.1016/j.bbcan.2010.02.004.
10. Arivalagan, K.; Ravichandran, S.; Rangasamy, K.; et al. Nanomaterials and its Potential Applications. *Int. J. ChemTech. Res.* **2011**, *3*, 534–538.
11. Khan, F.H. Chemical hazards of nanoparticles to human and environment (A review). *Orient. J. Chem.* **2013**, *29*, 1399–1408. https://doi.org/10.13005/ojc/290415.
12. Abdel-Mohsen, A.M.; Abdel-Rahman, R.M.; Hrdina, R.; et al. Antibacterial cotton fabrics treated with core-shell nanoparticles. *Int. J. Biol. Macromol.* **2012**, *50*, 1245–1253. https://doi.org/10.1016/j.ijbiomac.2012.03.018.
13. Barbhuiya, S.; Das, B.B.; Adak, D.; et al. Advancements in nano-engineering of cement and concrete: A comprehensive review. *Emerg. Mater.* **2025**, *8*, 5843–5882. https://doi.org/10.1007/s42247-025-01003-0.
14. Jang, Y.J.; Simer, C.; Ohm, T. Comparison of zinc oxide nanoparticles and its nano-crystalline particles on the photocatalytic degradation of methylene blue. *Mater. Res. Bull.* **2006**, *41*, 67–77. https://doi.org/10.1016/j.materresbull.2005.07.038.

15. Ganapathy Selvam, G.; Sivakumar, K. Phycosynthesis of silver nanoparticles and photocatalytic degradation of methyl orange dye using silver (Ag) nanoparticles synthesized from *Hypnea musciformis* (Wulfen) J.V. Lamouroux. *Appl. Nanosci.* **2015**, *5*, 617–622. https://doi.org/10.1007/s13204-014-0356-8.
16. Jangjoy, A.; Matloub, S. Optimizing carbon-based perovskite solar cells with pyramidal core–shell nanoparticles for high efficiency. *Plasmonics* **2025**, *20*, 265–275. https://doi.org/10.1007/s11468-024-02277-6.
17. Hammal, A.; Al-Qassabeen, B.S.; Hafez, K. Improving solar panel performance using a paraffin wax/copper oxide nanoparticle hybrid phase change material. *Sci. Rep.* **2025**, *15*, 37908. https://doi.org/10.1038/s41598-025-37908-8.
18. Mirzaei, H.; Darroudi, M. Zinc oxide nanoparticles: Biological synthesis and biomedical applications. *Ceram. Int.* **2017**, *43*, 907–914. https://doi.org/10.1016/j.ceramint.2016.10.051.
19. Khan, S.T.; Musarrat, J.; Al-Khedhairy, A.A. Countering drug resistance, infectious diseases, and sepsis using metal and metal oxides nanoparticles: Current status. *Colloids Surf. B Biointerfaces* **2016**, *146*, 70–83. https://doi.org/10.1016/j.colsurfb.2016.05.046.
20. Ghasemi, F.; Jalal, R. Antimicrobial action of zinc oxide nanoparticles in combination with ciprofloxacin and ceftazidime against multidrug-resistant *Acinetobacter baumannii*. *J. Glob. Antimicrob. Resist.* **2016**, *6*, 118–122. https://doi.org/10.1016/j.jgar.2016.04.007.
21. Sarsenov, S. Hollow CuO Microparticles for the Efficient Degradation of Model Pollutant Dyes. Master's Thesis, Nazarbayev University, Astana, Kazakhstan, 2022.
22. Nguyen, T.B.; Dong, C.D.; Huang, C.; et al. Fe-Cu bimetallic catalyst for the degradation of hazardous organic chemicals exemplified by methylene blue in Fenton-like reaction. *J. Environ. Chem. Eng.* **2020**, *8*, 104139. https://doi.org/10.1016/j.jece.2020.104139.
23. Gupta, A.; Khosla, N.; Govindasamy, V.; et al. Trimetallic composite nanofibers for antibacterial and photocatalytic dye degradation of mixed dye water. *Appl. Nanosci.* **2020**, *10*, 4191–4205. https://doi.org/10.1007/s13204-020-01540-6.
24. de Oliveira Guidolin, T.; Possolli, N.M.; Polla, M.B.; et al. Photocatalytic pathway on the degradation of methylene blue from aqueous solutions using magnetite nanoparticles. *J. Clean. Prod.* **2021**, *318*, 128556. https://doi.org/10.1016/j.jclepro.2021.128556.
25. Zhang, L. Photocatalysts with Adsorption Property for Dye-Contaminated Water Purification. PhD Thesis, The University of Queensland, Brisbane, Australia, 2017. https://doi.org/10.14264/uql.2017.864.
26. Nuramdhani, I. Towards Environmentally Benign Wastewater Treatment-Photocatalytic Study of Degradation of Industrial Dyes. Master's Thesis, University of Canterbury, Christchurch, New Zealand, 2011.
27. Mohamed, R.M.; Mkhalid, I.A.; Baeissa, E.S.; et al. Photocatalytic degradation of methylene blue by Fe/ZnO/SiO_2 nanoparticles under visible light. *J. Nanotechnol.* **2012**, *2012*, 329082. https://doi.org/10.1155/2012/329082.
28. Akpan, U.G.; Hameed, B.H. Parameters affecting the photocatalytic degradation of dyes using TiO_2-based photocatalysts: A review. *J. Hazard. Mater.* **2009**, *170*, 520–529. https://doi.org/10.1016/j.jhazmat.2009.05.039.
29. Kumar, S.A.; Jarvin, M.; Inbanathan, S.S.R.; et al. Facile green synthesis of magnesium oxide nanoparticles using tea (*Camellia sinensis*) extract for efficient photocatalytic degradation of methylene blue dye. *Environ. Technol. Innov.* **2022**, *28*, 102746. https://doi.org/10.1016/j.eti.2022.102746.
30. Ajmal, A.; Majeed, I.; Malik, R.N.; et al. Principles and mechanisms of photocatalytic dye degradation on TiO_2 based photocatalysts: A comparative overview. *RSC Adv.* **2014**, *4*, 37003–37026. https://doi.org/10.1039/c4ra06658h.
31. Khan, I.; Saeed, K.; Zekker, I.; et al. Review on methylene blue: Its properties, uses, toxicity and photodegradation. *Water* **2022**, *14*, 242. https://doi.org/10.3390/w14020242.
32. Kayabaşı, Y.; Erbaş, O. Methylene blue and its importance in medicine. *Demiroglu Sci. Univ. Florence Nightingale J. Med.* **2020**, *6*, 136–145. https://doi.org/10.5606/fng.btd.2020.25035.
33. Din, M.I.; Khalid, R.; Najeeb, J.; et al. Fundamentals and photocatalysis of methylene blue dye using various nanocatalytic assemblies—A critical review. *J. Clean. Prod.* **2021**, *298*, 126567. https://doi.org/10.1016/j.jclepro.2021.126567.
34. Yu, H.; Zhu, J.; Qiao, R.; et al. Facile Preparation and Controllable Absorption of a Composite Based on PMo12/Ag Nanoparticles: Photodegradation Activity and Mechanism. *ChemistrySelect* **2022**, *7*, e202103668. https://doi.org/10.1002/slct.202103668.
35. Feng, X.; Wang, B.; Gao, G.; et al. $Mn_yCo_{3-y}O_x$ bimetallic oxide prepared by ultrasonic technology for significantly improved catalytic performance in the reduction of NO_x with NH_3. *Fuel* **2023**, *352*, 129159. https://doi.org/10.1016/j.fuel.2023.129159.
36. Zhang, J.; Zhong, A.; Huang, G.; et al. Enhanced efficiency with CDCA co-adsorption for dye-sensitized solar cells based on metallosalophen complexes. *Sol. Energy* **2020**, *209*, 316–324. https://doi.org/10.1016/j.solener.2020.08.096.
37. Hu, J.; Zhao, L.; Luo, J.; et al. A sustainable reuse strategy of converting waste activated sludge into biochar for contaminants removal from water: Modifications, applications and perspectives. *J. Hazard. Mater.* **2022**, *438*, 129437. https://doi.org/10.1016/j.jhazmat.2022.129437.
38. Wang, Z.; Dai, L.; Yao, J.; et al. Enhanced adsorption and reduction performance of nitrate by Fe–Pd–Fe_3O_4 embedded multi-walled carbon nanotubes. *Chemosphere* **2021**, *281*, 130718. https://doi.org/10.1016/j.chemosphere.2021.130718.

39. Yasin, A.; Fatima, U.; Shahid, S.; et al. Fabrication of Copper Oxide Nanoparticles Using *Passiflora edulis* Extract for the Estimation of Antioxidant Potential and Photocatalytic Methylene Blue Dye Degradation. *Agronomy* **2022**, *12*, 2315. https://doi.org/10.3390/agronomy12102315.
40. Iqbal, S.; Amjad, A.; Javed, M.; et al. Boosted spatial charge carrier separation of binary $ZnFe_2O_4$/S-g-C_3N_4 heterojunction for visible-light-driven photocatalytic activity and antimicrobial performance. *Front. Chem.* **2022**, *10*, 975355. https://doi.org/10.3389/fchem.2022.975355.
41. Moosavi, S.; Li, R.Y.M.; Lai, C.W.; et al. Methylene blue dye photocatalytic degradation over synthesised Fe_3O_4/AC/TiO_2 nano-catalyst: Degradation and reusability studies. *Nanomaterials* **2020**, *10*, 2360. https://doi.org/10.3390/nano10122360.
42. Samsudin, E.M.; Goh, S.N.; Wu, T.Y.; et al. Evaluation on the photocatalytic degradation activity of reactive blue 4 using pure anatase nano-TiO_2. *Sains Malays.* **2015**, *44*, 1011–1019. https://doi.org/10.17576/jsm-2015-4407-13.
43. Alalwiat, A.A.; Khan, M.; Khan, S.; et al. Synthesis and characterization of a bulk-polymerized molecularly imprinted polymer for selective batch adsorption of Acid Yellow 76 dye from real water samples. *Int. J. Chem. React. Eng.* **2026**, *24*, 473–487. https://doi.org/10.1515/ijcre-2025-0231.
44. Khan, S.; Ajmal, S.; Hussain, T.; et al. Clay-based materials for enhanced water treatment: Adsorption mechanisms, challenges, and future directions. *J. Umm Al-Qura Univ. Appl. Sci.* **2025**, *11*, 219–234. https://doi.org/10.1007/s43994-023-00083-0.
45. Mahlaule-Glory, L.M.; Hintsho-Mbita, N.C. Green Derived Zinc Oxide (ZnO) for the Degradation of Dyes from Wastewater and Their Antimicrobial Activity: A Review. *Catalysts* **2022**, *12*, 833. https://doi.org/10.3390/catal12080833.
46. Elkady, M.F.; Hassan, H.S. Photocatalytic degradation of malachite green dye from aqueous solution using environmentally compatible Ag/ZnO polymeric nanofibers. *Polymers* **2021**, *13*, 2033. https://doi.org/10.3390/polym13132033.
47. Saleem, S.; Khalid, A.; Munir, M.A.; et al. A comprehensive role of co-doping (Ce, Al) in dielectric, magnetic, and optical properties of NiO for its efficient use in magneto-optical and spintronics device applications. *Ceram. Int.* **2025**, *51*, 4971–4987. https://doi.org/10.1016/j.ceramint.2024.11.469.
48. Mufti, N.; Pratiwi, N.I.; Kurniawan, R.; et al. ZnO/Ag thin film and reuse for Malachite Green degradation based on solar simulator. *AIP Conf. Proc.* **2023**, *2858*, 060011. https://doi.org/10.1063/5.0163573.
49. Hussain, A.; Fiaz, S.; Almohammedi, A.; et al. Optimizing photocatalytic performance with Ag-doped ZnO nanoparticles: Synthesis and characterization. *Heliyon* **2024**, *10*, e35725. https://doi.org/10.1016/j.heliyon.2024.e35725.
50. Onoriode-Afunezie, M.A.O.; Krutkevičius, J.; Šulčiūtė, A. Design and application of hetero-multicomponent metal oxide photocatalysts for wastewater treatment: Ti–Cu–Zn catalysts and future research directions. *Molecules* **2026**, *31*, 299. https://doi.org/10.3390/molecules31020299.
51. Jeong, S.H.; Choi, H.; Kim, J.Y.; et al. Silver-based nanoparticles for surface plasmon resonance in organic optoelectronics. *Part. Part. Syst. Charact.* **2015**, *32*, 164–175. https://doi.org/10.1002/ppsc.201400117.
52. Chen, Y.C.; Liu, B.Y.; Feng, Y.; et al. Light-induced antibonding orbital occupancy accelerates ion intercalation kinetics for enhanced capacitance of photo-rechargeable supercapacitor based on MnO_2/ZnO electrode. *J. Energy Storage* **2026**, *152*, 120610. https://doi.org/10.1016/j.est.2026.120610.